Superstructure ordering in lanthanum-doped lead magnesium niobate

D. M. Fanning and I. K. Robinson[a)]
Department of Physics, University of Illinois at Champaign–Urbana, Urbana, Illinois 61801-3080

S. T. Jung, E. V. Colla, D. D. Viehland, and D. A. Payne
Department of Materials Science and Engineering, University of Illinois at Champaign–Urbana, Urbana, Illinois 61801-3080

(Received 19 July 1999; accepted for publication 7 October 1999

Superstructure reflections of lead magnesium niobate (PMN , $Pb(Mg_{1/3}Nb_{2/3}O_3$, were measured with synchrotron radiation x-ray diffraction. Our data conclusively demonstrate that the $(h+\frac{1}{2},k+\frac{1}{2},l+\frac{1}{2})$-type reflections are the result of chemical ordering between the Mg and Nb ions in domains of 50 Å. Structure factor analysis of these peaks reveals an oxygen displacement within the ordered regions of 0.044(3 Å along a ⟨100⟩ direction towards the Nb ion. Single crystals of La-doped PMN (La–PMN exhibit much larger chemically ordered regions (up to 900 Å for 10% La–PMN . Structural analysis of the La–PMN suggests that as the ordered region increases in size, the ordering changes from complete Nb:Mg ordering and approaches $Nb:(Mg_{2/3}Nb_{1/3}$ ordering. Although anticipated from electrostatic energy arguments, our conclusions are based on a clear trend in the bond length of the mixed site as a function of La doping. © *2000 American Institute of Physics*. [S0021-8979(00 01302-5]

I. INTRODUCTION

Relaxor ferroelectrics are characterized by a frequency-dependent dielectric response which has a broad maximum as a function of temperature. In addition, relaxors possess a local polarization at temperatures well above their dielectric maximum. In contrast, ''normal'' ferroelectrics have a sharp phase transition at their Curie point, above which no polarization exists. The origin and explanation of this relaxor behavior is an ongoing research problem. The prototypical relaxor is lead magnesium niobate (PMN , or $Pb(Mg_{1/3}Nb_{2/3}O_3$, which was first synthesized by Smolenskii and Agranovskaya in the 1950s.[1] PMN has since found applications in multilayer capacitors, infrared devices, and other systems where its unique properties have been exploited, even if they are not perfectly understood. Of greatest interest is PMN's very high relative permittivity (~30 000 over a wide temperature range near room temperature.

PMN has the common ABO_3 cubic perovskite structure with Pb on the cube corners, Mg or Nb in the body-center position, and oxygen on the face centers. However, the finer points such as the size and direction of ion displacements within the perovskite model have not been as easy to deduce.[2–4] Compositional fluctuations exist on the nanometer scale and are believed to be responsible for PMN's very broad peak in dielectric constant versus temperature, which is also frequency dependent. Smolenskii[5] and others proposed that local inhomogeneities in chemistry and/or structure result in microdomains having a distribution of Curie temperatures, which accounts for the diffuse peak in the dielectric constant. The presence of a mixed B site and the random environment available to the lead atoms[4] have made a precise structure determination difficult, but progress is being made with the help of synchrotron sources.[6] Theoretical interpretations of relaxors have been offered using models of super paraelectric clusters,[7] an orientational glass,[8] and a quenched random field.[9] A helpful review was given by Ye.[10] The charge heterogeneity within PMN and its relation to the ferroelectric domains should help to understand the behavior of this relaxor.

The existence of a superstructure in PMN was first observed in selected area electron diffraction experiments.[11] Using a transmission electron microscope, superstructure spots were imaged at the $(h+\frac{1}{2},k+\frac{1}{2},l+\frac{1}{2})$ positions. Because the half-integer peaks are at the body-centered positions in the reciprocal lattice, the symmetry of the superstructure must have a face-centered-cubic arrangement within a doubled unit cell in real space $(Fm3m)$.

One type of model that would give superstructure peaks at the $(h+\frac{1}{2},k+\frac{1}{2},l+\frac{1}{2})$ positions is displacement ordering which gives a different pattern. In this class of models, atoms in adjacent unit cells are displaced in opposite directions, also producing a doubled unit cell. If the displacement is Δd, and adjacent atoms are displaced in opposite ⟨111⟩ directions, then the structure factors will have the form

$$F_{hkl} \propto f \sin(q\Delta d \quad \text{(when } h,k,l \text{ are all half integers .} \quad (1$$

The $|F|$ vs $|q|$ graph of the superstructure peaks would initially increase, passing a maximum when $q=\pi/(2\Delta d)$, and then decrease. This was the observation for PMN in the study by Zhang *et al.*,[12] and hence, they concluded that an ordering in the displacement of ions was producing the superstructure. However, they did not report a full structure determination.

Another model that could account for these superstructure peaks involves small regions of 1:1 chemical ordering of the B-site magnesium and niobium ions (Fig. 1 . This was first proposed in transmission electron microscopy (TEM

[a)] Electronic mail: ikr@uiuc.edu

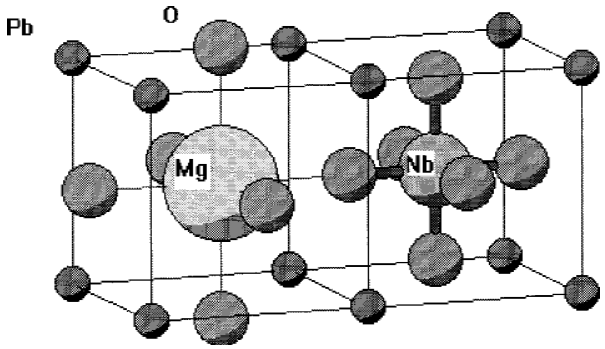

FIG. 1. Model of chemical ordering and oxygen ions displaced towards the Nb ion used in fitting.

studies.[13] The implied 1:1 ordering found in PMN is somewhat unexpected given the Mg:Nb stoichiometry of 1:2, but this nonstoichiometric ordering may help stabilize the perovskite over the pyrochlore phase in PMN.[14] The nonstoichiometric domains would be then embedded in a sea of Nb-rich domains. The ordered regions have a net negative charge which, it was proposed, restricts their size, even when the crystals are annealed. Chen, Chan, and Harmer provide evidence for this model in their study.[15] By doping with La^{3+}, they showed that the size of the ordered domains can be dramatically increased. The La^{3+} ion contributes an extra positive charge compared with the Mg^{2+}, thus lessening the charge restriction so the negatively charged ordered region can increase in size. The opposite effect was seen when doping with Na^{1+}.

A variation of the complete chemical ordering model that maintains the charge balance is the ''random layer'' model,[15] in which the 1:1 ordering is between two generic chemical species, B and B''. In this model, B contains a random occupation of Mg and Nb ions in a 2:1 ratio, while B'' is always Nb. Thus, the B site is disordered, while B'' is ordered, so the superstructure is well defined. In this extreme case, there would be no charge imbalance and the entire crystal volume could be composed of these ordered regions with the chemical formula: $Pb[(Mg_{2/3}Nb_{1/3\ 1/2}Nb_{1/2}]O_3$. Intermediate situations between the full 1:1 Mg:Nb chemically ordered model and the $B\ -B''$ model can exist, with different volume fractions of the ordered regions, depending on their exact compositions.

The above descriptions result when adjacent unit cells have one or more sites either occupied by different ions or with a preference for different types of ions. Effectively, this doubles the size of the unit cell, producing a superstructure. A diffraction experiment is a good way to probe the degree of ordering through crystallographic analysis of structure factor measurements. If the two B-site ions have effective atomic form factors f_{I} and f_{II}, then a simple derivation gives the form of the structure factors as a function of momentum transfer magnitude $|q|$:

$$F_{hkl} \propto f_{\mathrm{I}} - f_{\mathrm{II}} \quad \text{(when } h,k,l \text{ are all half integers . (2}$$

So, for both the 1:1 and $B\ :B''$ chemical ordering models, the intensity of the superstructure reflections depends on the difference in form factor of the two chemical species, and hence, gradually decrease as a function of momentum transfer $|q|$. In the complete chemical ordering model, this results in F_{hkl} being proportional to $f_{\mathrm{Nb}} - f_{\mathrm{Mg}}$. In the charge balanced version of the $B\ :B''$ chemical ordering model, the result is identical except for a factor of 2/3:

$$F_{hkl} \propto f_{\mathrm{Nb}} - (\tfrac{2}{3} f_{\mathrm{Mg}} + \tfrac{1}{3} f_{\mathrm{Nb}} = \tfrac{2}{3}(f_{\mathrm{Nb}} - f_{\mathrm{Mg}} \ , \qquad (3$$

which makes the two chemically ordered models (or any linear combination of them indistinguishable in the distribution of superstructure intensities, unless measurements are made on an absolute scale.

Evidence for the random layer model in $A(B_{1/3}B''_{2/3})\ O_3$ systems has recently been reported by Akbas and Davies[16] who found greatly increased ordered regions in $Pb(Mg_{1/3}Ta_{2/3}\ O_3$ and similar ceramics by annealing at 1325 °C. This is strong evidence that the random layer model applies to that system because the excess electrostatic energy in such highly ordered systems would make the space-charge model impossible (see Sec. VI below . However, similar annealing experiments for extended periods have so far failed to coarsen the ordered domains of PMN. Viehland *et al.*[17] also measured data supporting the random layer model in 10% La–PMN in a *Z*-contrast high-resolution TEM experiment. They were able to image columns of atoms in ordered regions and determine the chemical composition. However, their pure PMN measurements are inconclusive due to the fact that their sample thickness was 200 Å so that they were unable to image just the 50 Å ordered region.

By comparing the superstructure and bulk intensities, Lin and Wu[18] found in powder diffraction experiments that for La concentrations greater than 10%, there is maximum ordering on the B sites. They fit their data with a space-charge model over a given volume fraction, but the results would also fit a ''random layer'' model over a larger volume. However, at 10% La content and below, the superstructure peaks are very weak. Also, their plot of lattice constant versus La content (x fits a straight line for $x > 10\%$, suggesting complete solid solutions are formed between the La and Pb atoms. However, for x 10% the lattice constant deviates from the fit, suggesting a more complicated structure.

This article focuses attention on the concentration range below 10%, where the powder diffraction could not give reliable results on ordering. Single-crystal x-ray diffraction also allows us to determine the atomic structure of the ordered region. The organization of this article is as follows. We first describe the crystallographic analysis and the refinement of the structure. We then estimate the electrostatic energies involved with the various configurations and conclude that a purely electrostatic model (with complete chemical ordering will not explain the doping trends. An alternative analysis based on strain arguments finds that all the changes take place around the B (Mg site. From this we deduce the extent of a doping driven compositional modification at that site, and demonstrate that this is compatible with the electrostatic picture.

II. CRYSTAL GROWTH

Crystals of pure PMN (Ref. 19 of roughly 2 mm per side were used. One crystal was as grown, with well-formed ⟨100⟩ faces on three sides. The other was cut from a larger crystal and polished so that its largest face was ⟨110⟩. Lanthanum-doped crystals were grown for this experiment using high-temperature solution growth. First, La–PMN powder was prepared using the columbite method described by Swartz and Shrout.[20] Powders of PbO, MgO, Nb_2O_5, and La_2O_3 with purities exceeding 99.7% were used. When doping with La^{3+} for Pb^{2+}, it is necessary to account for the charge imbalance in one of two ways. By keeping the ratio of Mg:Nb concentration fixed, *A*-site vacancies can be introduced:

$$Pb_{1-3x/2}La_{x\quad x/2}(Mg_{1/3}Nb_{2/3}\ O_3,$$

where represents a vacancy. For our samples, however, we increased the Mg:Nb ratio to prevent *A*-site vacancies. The columbite was first produced by heating the magnesium and niobium oxides to 1000 °C for 6 h:

$$\frac{1+x}{3}MgO+\frac{2-x}{3}\frac{1}{2}Nb_2O_5 \quad Mg_{(1+x\ /3}Nb_{(2-x\ /3}O_{(4-x\ /2}. \tag{4}$$

This was then combined with appropriate amounts of La_2O_3 and PbO:

$$\frac{x}{2}La_2O_3+(1-x\ PbO+Mg_{(1+x\ /3}Nb_{(2-x\ /3}O_{(4-x\ /2}$$

$$La_xPb_{1-x}(Mg_{(1+x\ /3}Nb_{(2-x\ /3}\ O_3. \tag{5}$$

La–PMN powder was then formed by firing to 850 °C for 6 h. x-ray powder diffraction confirmed the resulting perovskite phase.

Single-crystal growth involved combining La–PMN powder with a flux. The amount of lead oxide flux ranged from one to one and a half times the weight of the PMN powder. The mixture was placed in a platinum crucible, which was tightly covered, and placed in a larger crucible. Alumina powder surrounded the platinum crucible to help prevent lead loss upon firing. A typical firing schedule involved rapid heating to 1250 °C, soaking for 12 h, then slow cooling at 2°/h to 1000 °C. Cooling continued at 5°/h to 800 °C, and then the mixture was brought to room temperature at 50°/h. We decided on these temperatures based on the PbO–PMN phase diagram published by Ye, Tissot and Schmid.[21] The residue was partially dissolved with boiling nitric acid, and single crystals were extracted. In all trials, only small crystals were found. The largest 3% La–PMN crystals were approximately 1 mm per side, while the 10% La–PMN crystals were only about 0.5 mm per side and some were black in color which may be due to Pt contamination from the crucible. The crystal growth was reproducible, as La–PMN crystals from different batches behaved similarly. However, the strength of superstructure peaks was found to decrease over a 12 month period, suggesting the crystals were slightly unstable.

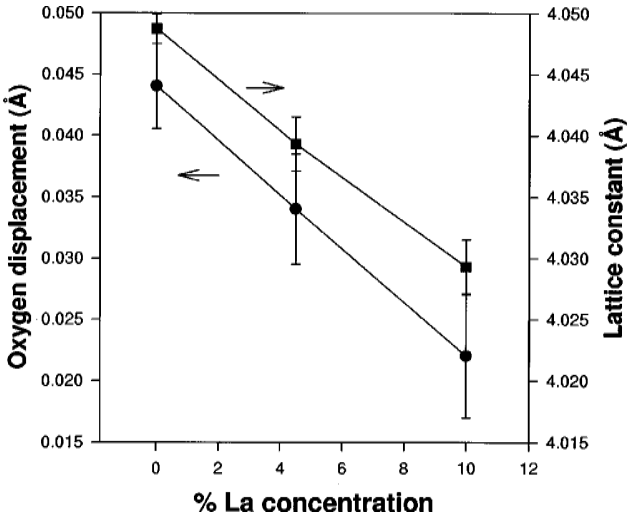

FIG. 2. Derived displacement of oxygen atoms toward niobium and overall lattice constant as a function of nominal La^{3+} concentration.

III. MEASUREMENTS

Each crystal was oriented on the diffractometer with one of its flat faces aligned nearly perpendicular to the phi axis.[22] This made it easier to estimate, and hence, correct for the beam's penetration through the crystal at any angle. Except for the ⟨110⟩ oriented crystal of pure PMN, this face was always close to a ⟨100⟩ orientation, which we designated (001 . Measurements were taken at Brookhaven National Laboratory's National Synchrotron Light Source on Beamline X16C. The incoming x-ray beam was tuned to 8.5 keV and focused onto a flat face of the PMN crystal. The beam was defined by slits to be 1×1 mm. The linear absorption coefficient for PMN at 8.5 keV is approximately 1150 cm^{-1}, giving a characteristic penetration depth of 8.7 μm along the beam direction. The detector arm's slits were set at 2 $\times2$ mm to define the resolution. We determined the orientation matrix of the crystal by measuring several bulk Bragg reflections. The refined lattice parameters were 4.048(2 Å for pure PMN, in agreement with published values.[23] A graph of average lattice constants versus percent La doping shows a steady decrease (Fig. 2 , and superimposes within error with the powder study of Lin *et al.*, but confirms the existence of an anomaly at small La concentrations.

Scans were then made to measure the integrated intensities of the $(h+\frac{1}{2},k+\frac{1}{2},l+\frac{1}{2})$ superstructure peaks. Because of the big differences in domain size, and hence peak profile, two different methods were needed. The well-ordered crystals (10% La doping used conventional rocking curves in theta, corrected for the Lorentz factor. The less well-ordered samples (including undoped were measured by reciprocal lattice scans varying one of the indices (Fig. 3 . These peaks were much broader than our resolution function, so it was necessary to integrate them in three dimensions. We initially took separate measurements along the *h, k*, and *l* directions, but found the widths (in reciprocal lattice units for each direction to be approximately constant, and independent of the direction scanned, so it was sufficient to scan in only one direction. The integrated intensity was measured as the area

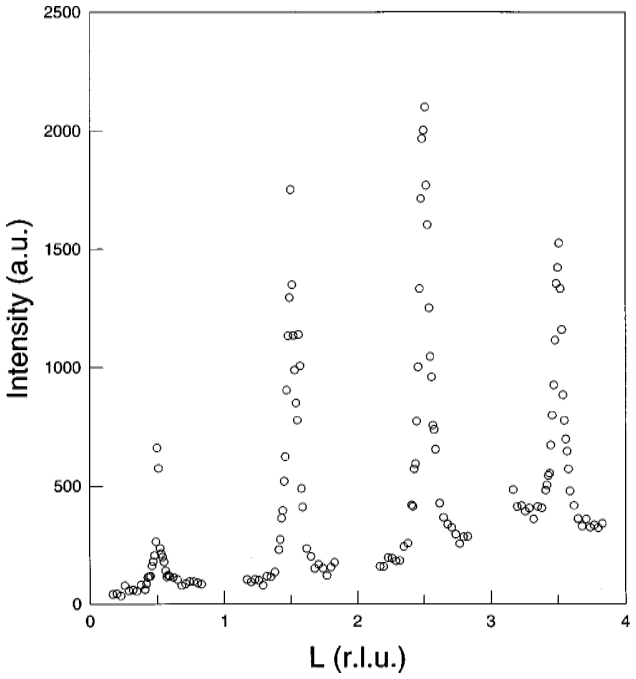

FIG. 3. Raw x-ray diffraction data showing the intensities of four adjacent (1/2,1/2,*L*) superstructure peaks scanned in the Miller index *L*.

under the peak minus the interpolated background. After adjusting for the counting time and the step size in h, the intensities were corrected for absorption as described in the following section. Taking the square root gives a measurement that is proportional to $|F|$. Reliable structure factor measurements of bulk peaks of perfect single crystals are complicated by extinction effects. Extinction is less of a problem in powder diffraction experiments; these have already been done on La–PMN,[18] as discussed above. However, for x less than 10%, the powder diffraction intensity of superstructure peaks is very low, and the study was inconclusive about structural information for the ordered domains. Because we were interested in extrapolation to the situation of pure PMN, we focused solely on this low concentration region.

Dielectric data were also measured for the La–PMN crystals. The dielectric response was measured using a Hewlett-Packard (HP 4284A inductance–capacitance–resistance (LCR bridge, which can cover a frequency range between 20 and 10^6 Hz. For low-temperature measurements, the samples were placed in a Delta Design 9023 test chamber. The temperature was measured using a HP 34401 A multimeter, via a platinum resistance thermometer mounted directly on the ground electrode of the sample fixture. Measurements were performed on cooling, using a rate of 2°/min at different frequencies. The results for the La-doped samples are presented in Fig. 4, taken between 1 and 500 kHz. By doping with La^{3+}, the ϵ (T) peak becomes broader and its maximum value decreases dramatically compared to pure PMN (Table I . Doping with La causes the peak in the dielectric constant to move to lower temperatures. Typical of relaxors, as the measurement frequency increases, the peak decreases and shifts to higher temperatures with dispersion

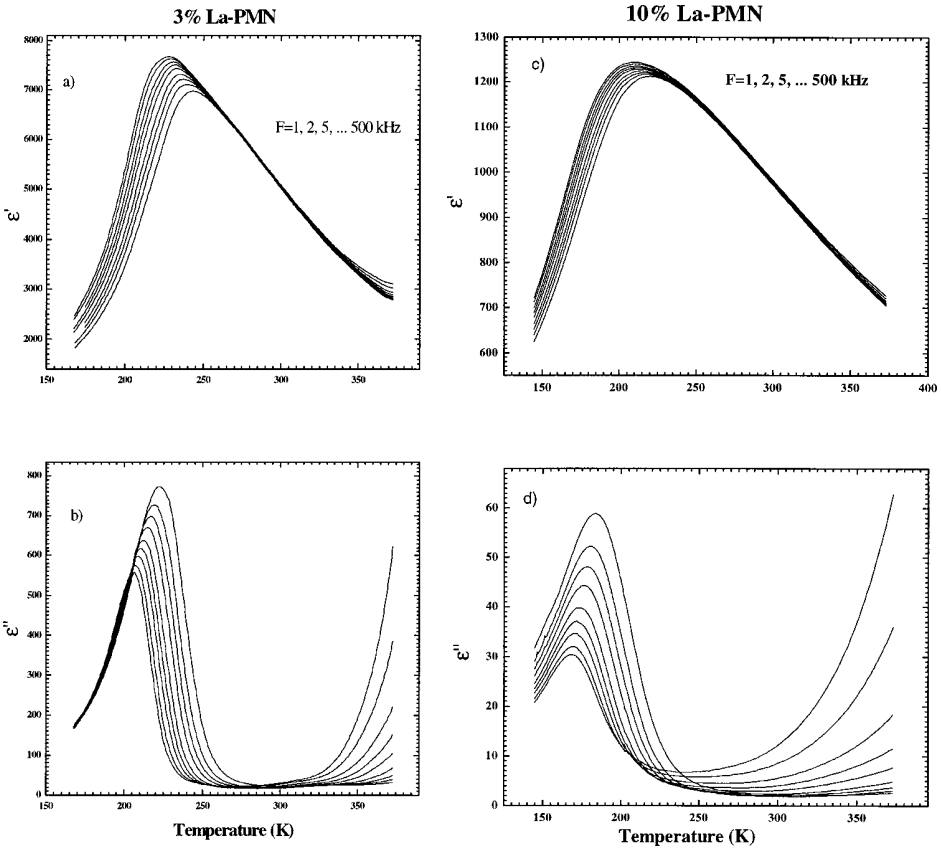

FIG. 4. Dielectric constant [(a and (c] and loss [(b and (d] measured on the 3% [(a and (b] and 10% [(c and (d] La–PMN samples as a function of temperature. Measurement frequencies ranges from 1 to 500 kHz and increase from left to right in each graph.

TABLE I. Summary of domain size and dielectric constant data measured for our samples with different La^{3+} doping concentrations. Increases in La^{3+} lead to much larger ordered regions and smaller dielectric constants.

Sample	Avg. FWHM ($Å^{-1}$	Domain size (Å	ϵ max. at 1 kHz	Temp. (K of ϵ max.
PMN ⟨100⟩	0.124	47		
PMN ⟨110⟩	0.118	50	29 995	268.0
3% La–PMN	0.0746	130	7 662	228.2
10% La–PMN	0.006 47	910	1243	210.0

in ϵ and ϵ''. ϵ decreases with increasing frequency on the low-temperature side of the peak, whereas ϵ'' increases with increasing frequency on the high-temperature side of the peak, characteristic of relaxor behavior. At higher temperatures (~ 350 K , the decrease in ϵ'' observed with increasing frequency can be attributed to thermally stimulated conductivity effects, i.e., charge transport rather than local charge displacements, possibly due to the small size of the crystals. The frequency dependence shows a slightly larger frequency dispersion than pure PMN, indicative of more relaxor-like behavior. Our results (except at high temperatures are consistent with the powder measurements of Chen, Chan, and Harmer[15] who measured 5% and 10% La–PMN. Together with our measured lattice constants, we believe this indicates our nominal La composition is roughly the actual composition.

IV. ANALYSIS

The symmetry and structure of the parent crystal is assumed to be ideal cubic perovskite (O_H^1). Here, we are concerned with the nature of the superstructure, evidenced by the intensities of the additional reflections. We continue to assume cubic symmetry because there is no evidence to indicate this is broken. By crystallographic analysis of peaks of the form $(h+\frac{1}{2},k+\frac{1}{2},l+\frac{1}{2})$, we attempted to determine the nature of the superstructure, and hence, determine the mechanism of ordering. We measured approximately 150 such reflections in total for each crystal. For each reflection, at least four symmetrically equivalent peaks were measured. We only looked at peaks with $\chi>30°$ (Ref. 22 to keep the entrance and exit beams passing through the alignment face. This only reduces the number of symmetrically equivalent peaks. By averaging over the symmetrically equivalent scans, the 150 measured peaks (out of a possible 300 were reduced to 19 crystallographically distinct reflections (of a possible 21 below the 2θ limit . This is a sufficient number to determine the basic structure of the ordered regions and observe changes with La doping. The agreement within the symmetry equivalent peaks was best for the larger pure PMN crystals at 7.8%. For 3% La–PMN, it was 14.1% and for 10% La–PMN, 18.1%. The larger errors are most likely due to the smaller crystal size and ill-defined faces which introduced errors through the absorption correction.

No conclusions can be drawn about the local symmetry of the superstructure because no reflections were found to be absent. The general shape of our raw data agrees with that of Zhang *et al.*,[12] in that it appears to show a sinusoidal variation with $|q|$ (Fig. 3 . However, there are important corrections needed to deduce structure factors from the raw data, which change the conclusions significantly. The absorption of the beam as it passes through the (Pb-rich sample must be accounted for. The size of the beam (~1 mm is slightly smaller than our pure PMN crystals and larger than the La-doped samples. At angles above a threshold incidence angle, the entire beam hits the pure PMN crystal. This is the extended face regime in which the integrated intensity is shown by Warren[24] to be proportional to

$$\int_{z=0}^{\infty} e^{-2\mu z/\sin\theta}\frac{A_0\ dz}{\sin\theta}. \qquad (6$$

This assumes an ''infinitely'' thick crystal and a beam whose footprint is smaller than the crystal's horizontal dimension. Here, μ is the absorption coefficient, A_0 is the area illuminated, θ is the incident angle, and z is the penetration of the beam into the crystal. The integral evaluates to $\frac{1}{2}\mu$, so the effect of absorption is just a constant factor because even though it increases with increasing path length at smaller incidence angles, the illiuminated area of the crystal increases.

However, below that threshold angle (and at all angles for the smaller crystals , the extended face geometry is no longer valid because the beam footprint is now larger than the crystal. The absorption must be accounted for by adjusting for the fraction of the beam that is illuminating the crystal which depends on the incidence angle α_i . This illumination correction is given by $1/\sin(\alpha_i)$, or $1/\sin(\theta)\sin(\chi)$, which is the footprint of the beam on the sample following the angle convention of Busing and Levy[22] and assuming the flat face of the sample is perpendicular to the phi axis, which was assured optically. This correction is significant for structure factors measured at low incidence angles. The extended face absorption correction has to be adjusted because some fraction of the beam never hits the crystal. This absorption correction is only valid for crystals with a flat face, and when the x rays that reach the detector enter and exit through that face symmetrically, $\alpha_i=\alpha_f$, as was the case in our measurements. Because of the large absorption of PMN, most radiation entering a side of the crystal would not contribute to the intensity anyway. Initially, we studied the smaller 10% La–PMN crystals in their as-grown, jagged state. Large errors were found in the scattering intensities in that symmetrically equivalent peaks had very different intensities. By polishing the crystal down to a flat face, this problem was largely eliminated.

The width of an x-ray peak is inversely proportional to the size of the domain that is contributing to that particular

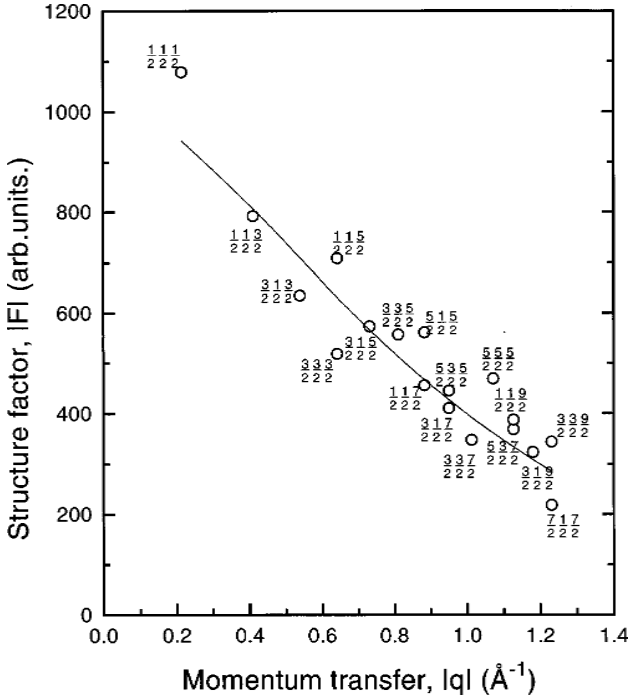

FIG. 5. X-ray structure factors of superstructure reflections for pure PMN. The fit is to a simple chemical ordering model.

scattering event as given by the Scherrer formula:

$$L = 0.94 \frac{2\pi}{\Delta q_{\mathrm{FWHM}}}, \qquad (7$$

where L is the characteristic length of the ordered region and Δq_{FWHM} is the peak width measured in reciprocal space. By measuring the width of half-order superstructure peaks, it is, therefore, possible to estimate the size of the ordered region. The average size of the domains that caused the superstructure peaks was 48 Å for both pure PMN samples, based on an average width of 0.12 Å^{-1}. The peak widths for various reflections were constant when measured in momentum transfer units (rather than angle , which indicates that the width is entirely a finite-size effect and has little contribution from the sample mosaic spread. For the La-doped case, we found there was a dramatic increase in ordered domain size with increasing La doping (Table I . Rough, quantitative agreement is found with the domain size and dielectric constant results of Chen, Chan, and Harmer's powder measurements.[15] The 10% La concentration produced ordered regions of approximately 900 Å. The peaks were so narrow that we were close to the limits of resolution and mosaic, which is why the θ-scan integration method was used.

V. RESULTS

The absorption/illumination corrected data show a very different q dependence from the raw data (Fig. 5 . The graph of structure factor versus $|q|$ follows the monotonic decay of the form factor that is characteristic of the chemical ordering models. This was true for both the pure PMN and the La-doped crystals that we studied. Using a simple chemical ordering model, it is possible to fit the general shape of the data (line in Fig. 5 . However, chemical ordering alone gives the smooth line of the form factor difference between Mg^{2+} and Nb^{5+} [Eq. (2], and is not able to explain the small, systematic variations seen in the data. For example, certain pairs of reflections, with different indices but the same magnitude of $|q|$, have different structure factors. This results in a large χ^2 of 3.6.

By varying the position or shape of the oxygen octahedra that surround the B sites, it was possible to fit the deviations from a smooth curve. One such model, with $R\bar{3}m$ symmetry, was suggested by Husson, Chubb, and Morell[25] and employed by Chen, Li, and Wang[26] in their extended x-ray absorption fine-structure study of PMN and other perovskites. We found that this model is consistent with our data as well for both the pure and the La-doped PMN. For the sake of simplicity, we assumed complete 1:1 chemical ordering between the B-site ions within each ordered region, but the model would apply equally well to the charge balanced $B - B''$ model (since the structure factors only differ by a multiplicative factor as explained above . Since we have no absolute scale factor in our model and the oxygen displacement is a small perturbation of the structure, we cannot determine the degree of 1:1 ordering on an absolute scale. In our model, the oxygen atoms move towards the smaller Nb^{5+} ions along a {100} axis (and hence, move away from the Mg^{2+} ions (Fig. 1 . This oxygen displacement enabled the model to fit variations in the structure factor for reflections that have the same magnitude of $|q|$, for example, reflections (1.5, 1.5, 1.5 and (0.5, 0.5, 2.5 . By fitting only the size of this oxygen displacement and assigning Debye–Waller factors to the Mg/Nb and O atoms, we found an optimal oxygen displacement of 0.044(3 Å for pure PMN (Fig. 6 . The improved fit has a χ^2 of only 0.6. We also tried models involving rotations of the oxygen octahedra, but these did not improve our fit. Using the same model for the doped crystals, we measure oxygen displacements as shown in Fig. 2 and found a χ^2 of 0.9 for 3% La–PMN and 1.2 for 10% La–PMN. The direction of the displacement is towards the smaller Nb ions, as expected. Due to the low sensitivity of x rays to oxygen, additional oxygen rotations cannot be ruled out, but our observed shrinking of oxygen displacements with increasing La is the main result.

We see contributions from the Pb and O only to the extent that they contribute to the ordering. Thus, we are only sensitive to displacements of Pb (and B-site ions that follow the alternating pattern of the 1:1 ordering, and even then, only by breaking the cubic symmetry and forming domains. We did not find any evidence for this in models that tested for antiparallel displacements of Pb or B-site ions.

Our results indicate that chemical ordering is the dominant cause of PMN's superstructure peaks. The ordered domains have an average size of 48 Å per side and are not strongly anisotropic, so we can assume they are roughly cubic in shape. These chemically ordered regions are believed to be distinct from PMN's nanopolar domains because they have different characteristics. The superstructure peaks that arise from them showed no response to applied electric fields of up to 2 kV/cm in our experiments, and they are also un-

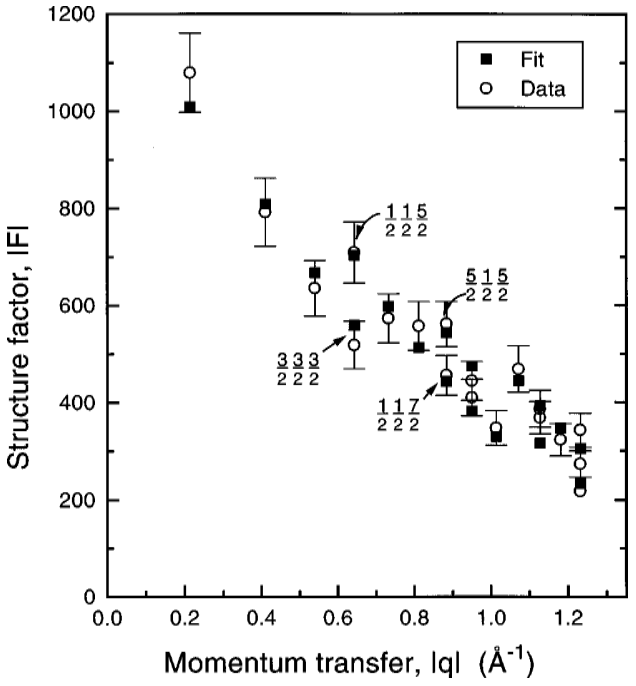

FIG. 6. Data of pure PMN fit with the oxygen displacement model. Four indices are indicated to show how the addition of the oxygen displacements makes it possible to fit different indices at the same $|q|$.

affected by temperature up to 970 °C.[27] The nanopolar domains, which appear when PMN is cooled, grow to about 100 Å at 5 K (Ref. 2 and are responsible for PMN's ferroelectric properties. Chemically ordered domains are not affected by temperature, increase with La doping and their growth causes a decrease in the dielectric response (Fig. 4 . A better understanding of the interaction between the two types of domains may help explain PMN's relaxor behavior.

VI. CHARGE IMBALANCE MODELS

Of course, the model of complete chemical ordering is only possible for limited domain sizes because there is, in fact, twice as much Nb as Mg in the chemical composition of PMN. More importantly, the Mg:Nb 1:1 stoichiometry leaves a net charge per unit cell of $-0.5e$. Assuming the domain shape is cubic, we can calculate the net charge of the cube:

$$\text{Volume}=h^3, \quad Q=\left(\frac{h}{a_0}\right)^3(-0.5e \ . \tag{8}$$

This net negative charge can be balanced by a surface layer of positive charge on the unit cells that enclose the ordered region. If such a layer were made up of unit cells of $PbNbO_3$, then each surface unit cell would have a net positive charge of $+e$. By setting the surface layer charge equal to the volume charge, we find that 12 unit cells along each cube dimension are needed to achieve charge balance:

$$\left(\frac{h}{a_0}\right)^3(0.5e \ =6\left(\frac{h}{a_0}\right)^2(1.0e \ , \quad \frac{h}{a_0}=12. \tag{9}$$

With a lattice constant of 4.05 Å, this region would be 48.6 Å per side. Thus, we conclude that our observed domain size of 48 Å is the minimum necessary so that one monolayer of unit cells of $PbNbO_3$ will counterbalance it. If this model is correct, we could conclude that these domains do not grow larger because they are strongly restricted by Coulombic forces.

The amount of electrostatic energy contained in such a charge imbalanced region of a crystal can be calculated in a straightforward manner.[28] Consider a spherical volume of radius R containing a total charge Q uniformly distributed in a medium of relative dielectric constant ϵ_r. Again, we assume a skin charge which counterbalances the volume excess charge, and hence, cancels all fields outside the sphere. The electrostatic energy is given by

$$U=\frac{1}{10}\frac{Q^2}{4\pi\epsilon_0\epsilon_r R}. \tag{10}$$

Now, if there are N^3 unit cells in the volume, each with an excess charge q, then $Q=N^3q$ and $R=Na_0$. Substituting gives

$$U=\frac{1}{10}\frac{(N^3q)^2}{4\pi\epsilon_0\epsilon_r(Na_0)}=\frac{1}{10}N^5\frac{q^2}{4\pi\epsilon_0\epsilon_r a_0}. \tag{11}$$

The energy per unit cell is then given by

$$u=\frac{U}{N^3}=\frac{1}{10}\frac{N^2}{\epsilon_r}\left(\frac{q}{e}\right)^2(3.6 \text{ eV} \ . \tag{12}$$

This gives $(13/\epsilon_r)$ eV per unit cell in pure PMN, assuming $N=12$ unit cells in the ordered region and complete chemical ordering $(q=0.5e)$. Considering ϵ_r may be quite large, this energy is certainly not unreasonable on the scale of typical cohesive energies of ionic solids. The actual value of ϵ_r, which is the relative dielectric constant of the ordered region, is not known, but an approximation of about 100 can be made using the Curie–Weiss law at PMN's growth temperature, resulting in $u\sim 0.13$ eV/unit cell for full chemical ordering in pure PMN.

It was proposed[15] that doping the Pb^{2+} sites with La^{3+} provides enough additional positive charge to allow these regions to become larger. However, at the quantitative level, we see that doping with La does not provide enough positive charge to account for the rapid increase in the ordered domain size. If we assume that the La is distributed evenly on the A sites, then the net charge for one formula unit of $La_xPb_{1-x}Mg_{0.5}Nb_{0.5}O_3$ is $(x-0.5)$ electrons per unit cell. As above, we find the number of unit cells per side of the ordered region:

$$\left(\frac{h}{a_0}\right)^3(0.5-x \ e=6\left(\frac{h}{a_0}\right)^2(1.0e \ , \quad \frac{h}{a_0}=\frac{6}{0.5-x}, \tag{13}$$

which has a weak dependence on x, giving only 15 unit cells, or 61 Å for 10% La doping, which is no where near the observed 1000 Å. It is possible that La goes preferentially into the ordered regions during growth, but no evidence for this was seen in comparing the positions of bulk and superstructure peaks.

We can draw the conclusion that the random layer model is valid for sufficient La concentrations, but the space-charge model is possible in the range below 10%. Also, we note that

TABLE II. Ionic radii from Shannon.[a]

	Charge	Coord.	Radius (Å
Pb	+2	12	1.50
La	+3	12	1.32
Mg	+2	6	0.72
Nb	+5	6	0.64
O	−2	2	1.35

[a]See Ref. 29.

the anomalous variation of lattice constant for La concentration less than 10% in the measurements of Lin and Wu[18] may also indicate a transformation from space-charge to random layer ordering.

VII. IONIC CONTACTS

A comprehensive explanation for why PMN chemically orders has not yet been given. We believe that strain plays an important role. In perovskites, there is a delicate balance between ionic contacts at the *A* site and at the *B* site. The relevant ionic radii, which vary with effective ionic charge and coordination number, are given in Table II.[29] In pure PMN, the lattice constant is 4.048 Å which, after accounting for two oxygen radii of 1.35 Å, leaves enough room to accommodate a *B*-site ion of radius 0.674 Å or smaller. Thus, the Nb^{5+} ion fits easily, but the Mg^{2+} ion is too large. However, if we construct a linear array of Nb^{5+} and Mg^{2+} ions (as in a 1:1 chemically ordered model and displace the oxygen atoms towards the smaller Nb ion, then the Mg ion can be comfortably accommodated. Our observation of oxygen displacements is entirely consistent with this model. The combination of chemical ordering, with the associated oxygen displacements, may lower the total energy by reducing the strain and thereby drive the 1:1 chemical ordering. Doping with La^{3+} decreases the lattice constant, thereby increasing the overall strain. This could make the chemically ordered state even more advantageous in energy and result in increased ordering.

As the overall lattice constant decreases with increased La^{3+} content, we observe that the size of the oxygen displacement also decreases (Fig. 2 . Both curves are on the same vertical scale, allowing us to observe that the two values change at an approximately equal rate. Using a hard-sphere model and the ionic radii (Table II , we see the O–Nb–O requires 3.98 Å and O–Mg–O requires 4.14 Å. In pure PMN, using our measured oxygen displacement, the O–Nb–O bond length is 3.96 Å, and the O–Mg–O bond length is 4.14 Å, so that the Nb ion is being squeezed slightly, but the Mg ion fits exactly. As La is added, we see from the data in Fig. 1 that the measured O–Nb–O bond length remains approximately constant at 3.97 Å, while the O–Mg–O bonds become progressively more compressed. The displacements are such that the O–Nb–O distance is roughly constant, and all of the strain is concentrated in the O–Mg–O bond (Fig. 7 .

This result makes little sense in the context of a fully 1:1 Mg:Nb chemically ordered model. It makes more sense if the

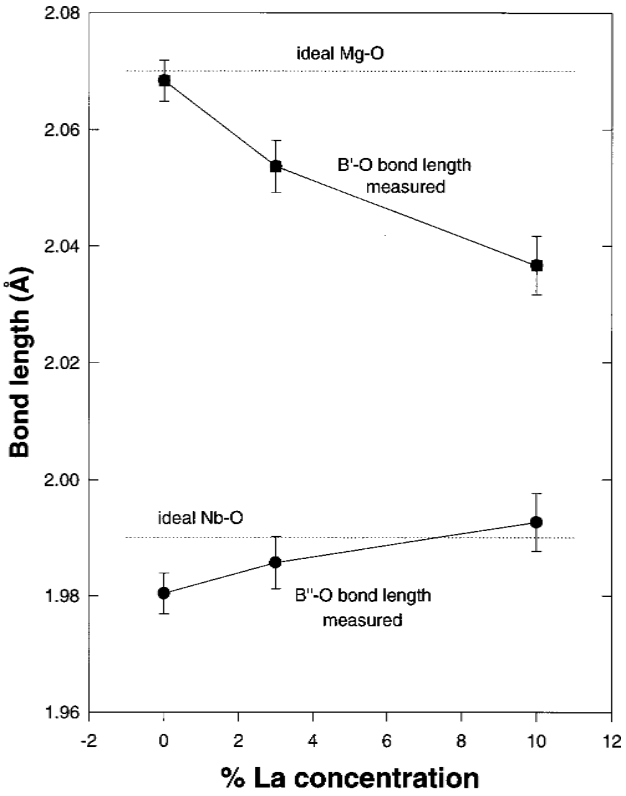

FIG. 7. Measured bond lengths of O–B –O and O–B''–O as a function of La^{3+} doping. The oxygen displacement is away from Mg^{2+} and towards Nb^{5+}, giving rise to the two bond lengths. The dotted lines indicate the ''ideal'' bond lengths of Mg–O and Nb–O using the ionic radii data (from Ref. 29 .

B , or ''Mg,'' site is showing a change of composition with La doping. The smaller bond length may force the larger Mg out of the B site, increasing the amount of Nb on B . This brings the ordered regions closer to neutral charge because of the additional positive charge carried by Nb^{5+} on the B site. In other words, the ordered region changes from complete Nb:Mg ordering in pure PMN and becomes closer to Nb:($Mg_{2/3}Nb_{1/3}$ ordering in 10% La–PMN. By this mechanism, the domain size is no longer limited by space charge and can grow larger. Also, because of the quadratic dependence of u on N [Eq. (13], the electrostatic energy becomes prohibitively large when N becomes larger. Hence, the charge redistribution on the B sites is necessary to accommodate large ordered domains in La–PMN.

Our data can be interpreted using the model of changing stoichiometry to accommodate the shrinking B site. Using the measured lattice constants a_0 and oxygen displacements D_{Oxy}, the space allowed for the B ion R_B is simply

$$R_B = a_0/2 - R_{\mathrm{oxygen}} + D_{\mathrm{oxy}}, \qquad (14$$

where R_{oxygen} is taken from Table II. A linear combination of the ionic radii R_{Mg} and R_{Nb} results in an effective radius. An independent estimate of the B occupancy is made by calculating the fractions of Mg and Nb that result in an ion that matches the measured size:

$$R_B = yR_{\mathrm{Mg}} + (1-y\ R_{\mathrm{Nb}}, \quad \text{giving} \quad y = \frac{R_B - R_{\mathrm{Nb}}}{R_{\mathrm{Mg}} - R_{\mathrm{Nb}}}. \qquad (15$$

TABLE III. R_B is the measured ionic radius that would fit in the B site. The fraction of Mg^{2+}, in combination with Nb^{5+}, that corresponds to that size and the resultant excess charge per unit cell are shown.

% La	R_B measured [Eq. (14]	Mg fraction on B site, y calc. [Eq. (15]	Charge/unit cell q/e calculated
0	0.718±0.003	0.98±0.04	−0.46±0.06
3	0.704±0.004	0.79±0.06	−0.19±0.08
10	0.688±0.005	0.60±0.08	+0.10±0.12

The results (Table III show good agreement for the pure PMN and 3% La–PMN, which have Mg occupancies of 0.98 and 0.79, respectively. For the 10% La–PMN, the Mg occupancy actually drops below 2/3 (which would make the region positively charged , but the value 2/3 is still within our error estimate.

VIII. CONCLUSION

We have found that PMN's superstructure peaks give an x-ray diffraction pattern that, when corrected for absorption and illumination, shows decreasing structure factors with increasing $|q|$. This leads us to conclude that chemical ordering is the dominant feature in PMN that causes its superstructure. We were able to further refine the positions of the oxygen atoms, and find their displacements to be towards the Nb ions and away from the Mg, or $(Mg_{2/3}Nb_{1/3})$, ions. While the increase in positive charge that La provides may facilitate the growth of 1:1 chemically ordered regions, we propose that strain effects and increased occupancy of Nb on the B site are also important. Since an increase in the ordered region size reduces PMN's maximum dielectric constant, we conclude that the chemically ordered region is not ferroelectrically active.

We propose a four-step model to explain the overall picture of chemical domain formation in PMN. In pure PMN, complete chemical ordering of Mg and Nb on the B sites is possible, from both an electrostatic and strain point of view. The first consequence of doping with the smaller La^{3+} on the Pb^{2+} site is a decrease in the lattice constant. Next, the O–Nb–O bonds remain roughly constant with doping, with all compression taking place at the B site. Third, this added strain forces some Mg ions out of the B site, making it richer in Nb on average. Finally, the combination of extra charge from La^{3+} on the A site and additional Nb^{5+} on the B site results in the ordered domain unit cells being closer to neutral charge and reduces the electrostatic energy. Therefore, the ordered domain sizes can grow larger with La^{3+} doping, as observed.

ACKNOWLEDGMENTS

This work was supported by DOE under Contract No. DEFG02-96ER45439 through the University of Illinois Materials Research Laboratory (MRL . The data were taken at the National Synchrotron Light Source, supported by DOE under Contract No. DEAO02-98CH10886.

[1] G. A. Smolenskii and A. I. Agranovskaya, Sov. Phys. Tech. Phys. **3**, 1380 (1958 .
[2] N. de Mathan, E. Husson, G. Calvarin, J. R. Gavarris, A. W. Hewat, and A. Morell, J. Phys.: Condens. Matter **3**, 8159 (1991 .
[3] A. Verbaere, Y. Piffard, Z. G. Ye, and E. Husson, Mater. Res. Bull. **27**, 1227 (1992 .
[4] S. G. Zhukov, V. V. Chernyshev, L. A. Aslanov, S. B. Vakhrushev, and H. Schenk, J. Appl. Crystallogr. **28**, 385 (1995 .
[5] G. A. Smolenskii, J. Phys. Soc. Jpn. **28**, 26 (1970 .
[6] H. D. Rosenfeld and T. Egami, Ferroelectrics **164**, 133 (1995 ; H. You, Q. M. Zhang, Phys. Rev. Lett. **79**, 3950 (1997 ; T. Egami, W. Dmowski, S. Teslic, P. K. Davies, I. W. Chen, and H. Chen, Ferroelectrics **206**, 231 (1998 .
[7] L. E. Cross, Ferroelectrics **76**, 241 (1987 .
[8] D. Viehland, M. Wuttig, and L. E. Cross, Ferroelectrics **120**, 71 (1991 .
[9] V. Westphal, W. Kleemann, and M. D. Glinchuk, Phys. Rev. Lett. **68**, 847 (1992 .
[10] Z.-G. Ye, Ferroelectrics **184**, 193 (1996 .
[11] H. B. Krause, J. M. Cowley, and J. Wheatley, Acta Crystallogr., Sect. A: Cryst. Phys., Diffr., Theor. Gen. Crystallogr. **35**, 1015 (1979 .
[12] Q. M. Zhang, H. You, M. L. Mulvihill, and S. J. Jang, Solid State Commun. **97**, 693 (1996 .
[13] A. D. Hilton, C. A. Randall, D. J. Barber, and T. R. Shrout, Ferroelectrics **93**, 379 (1989 ; I. A. Bursill, H. Qian, J.-L. Peng, and X.-D. Fan, Physica B **216**, 1 (1995 .
[14] D. D. Viehland and J.-F. Li, Ferroelectrics **158**, 381 (1994 .
[15] J. Chen, H. M. Chan, and M. P. Harmer, J. Am. Ceram. Soc. **72**, 593 (1989 .
[16] M. A. Akbas and P. K. Davies, J. Am. Ceram. Soc. **80**, 2933 (1997 .
[17] Y. Yan, S. J. Pennycook, Z. Xu, and D. D. Viehland, Appl. Phys. Lett. **72**, 3145 (1998 .
[18] L.-J. Lin and T.-B. Wu, J. Am. Ceram. Soc. **73**, 1253 (1990 .
[19] Commercially puchased, grown by Czochralski method.
[20] S. L. Swartz and T. R. Shrout, Mater. Res. Bull. **17**, 1245 (1982 .
[21] Z.-G. Ye, P. Tissot, and H. Schmid, Mater. Res. Bull. **25**, 739 (1990 .
[22] The standard angle conventions for a four-circle diffractometer are given in W. R. Busing and H. A. Levy, Acta Crystallogr. **22**, 457 (1967 .
[23] N. de Mathan, E. Husson, and A. Morell, Mater. Res. Bull. **27**, 867 (1992 .
[24] B. E. Warren, *X-Ray Diffraction* (Addison-Wesley, Reading, MA, 1969 .
[25] E. Husson, M. Chubb, and A. Morell, Mater. Res. Bull. **23**, 357 (1988 .
[26] I. W. Chen, P. Li, and Y. Wang, J. Phys. Chem. Solids **57**, 1525 (1996 .
[27] A. D. Hilton, D. J. Barber, C. A. Randall, and T. R. Shrout, J. Mater. Sci. **29**, 3461 (1990 .
[28] D. J. Griffiths, *Introduction to Electrodynamics* (Prentice-Hall, Englewood Cliffs, NJ, 1989 .
[29] R. D. Shannon, Acta Crystallogr., Sect. A: Cryst. Phys., Diffr., Theor. Gen. Crystallogr. **32**, 751 (1976 .